

AFeO₃ (A = La, Nd, Sm) and LaFe_{1-x}Mg_xO₃ perovskites: structural and redox properties

Piero Porta^{a,*}, Stefano Cimino^b, Sergio De Rossi^a, Marco Faticanti^a,
Giuliano Minelli^a, Ida Pettiti^a

^a Centro di Studio del CNR su “Struttura e Attività Catalitica di Sistemi di Ossidi” (SACSO), c/o Dipartimento di Chimica,
Università “La Sapienza”, Piazzale A. Moro 5, 00185 Rome, Italy

^b Dipartimento di Ingegneria Chimica, Università “Federico II”, Naples, Italy

Received 13 October 2000; received in revised form 1 December 2000; accepted 18 December 2000

Abstract

The synthesis and properties of polycrystalline AFeO₃ (A = La, Nd, Sm) and LaFe_{1-x}Mg_xO₃ (x = 0.0, 0.1, 0.2, 0.3, 0.4, and 0.5) perovskites prepared at different temperatures (623, 773, 923 and 1073 K) from decomposition of citrate precursors are reported. Chemical analysis, X-ray diffraction (XRD) for phase analysis, lattice parameters and crystallite dimension, BET surface area determination, diffuse reflectance spectroscopy, and magnetic susceptibility measurements were employed for the characterization of the solids. The reducibility of the samples was followed by temperature programmed reduction (TPR) and by reduction with in situ XRD. The calcination at different temperatures revealed that samples having less disordered perovskite structure are more easily formed. The variation of lattice constants and the order of reducibility within the AFeO₃ perovskites, LaFeO₃ > NdFeO₃ > SmFeO₃, have been linked to different Fe–O bond strength. A certain fraction of Fe⁴⁺ was observed by redox titration and TPR to be present in AFeO₃ perovskites, which, for charge balance, have small cation defectivity. The fraction of Fe⁴⁺ increases with the increase of x in LaFe_{1-x}Mg_xO₃ solid solutions. However, the Fe⁴⁺/Mg²⁺ ratio never reaches unity, so that these mixed perovskites, to preserve charge neutrality, contain oxygen defectivity. After reduction, all samples preserve the perovskite structure and the expansion of the unit cell volume in the reduced LaFe_{1-x}Mg_xO₃ perovskites is due to the higher content of larger Fe³⁺ species formed by reduction of Fe⁴⁺. The decreasing reducibility of LaFe_{1-x}Mg_xO₃ solid solutions at the increase of x has been correlated with oxygen atoms more strongly bonded. Optical and magnetic properties are also reported and discussed. © 2001 Elsevier Science B.V. All rights reserved.

Keywords: Perovskite oxide solid solutions; (La, Sm, Nd) iron perovskites; La (Mg, Fe) perovskites; Fe⁴⁺-containing perovskites

1. Introduction

Due to their variable structure and chemical composition, perovskite-type oxide materials of general formula ABO₃ have so far attracted great interest in many applied and fundamental areas of solid state chemistry, physics, advanced materials, and catalysis [1,2].

Many metals are stable in the ABO₃ perovskite structure provided that the A (usually a rare-earth metal in 12-coordination) and B (usually a transition metal in octahedral symmetry) cations have dimension ($r_A > 0.90 \text{ \AA}$, $r_B > 0.51 \text{ \AA}$) in agreement with the limits of the so-called “tolerance factor” t ($0.8 < t < 1.0$) defined by Goldschmidt [3], as $t = (r_A + r_O) / \sqrt{2}(r_B + r_O)$, where r_A , r_B , and r_O are the ionic radii for A, B, and O, respectively.

The high stability of the perovskite structure allows the partial substitution of either one or both A and B site cations by other metals with different oxidation state and consequent creation of structural defects, e.g. anionic or cationic vacancies [4,5]. For instance, upon substitution of B³⁺ transition metal cations by an ion preferentially stable in an oxidation state lower than 3+, the charge compensation is achieved, when possible, by oxidation of the B ion or by a decrease in the oxygen content of the perovskite with the eventual appearance of oxygen vacancies.

A systematic work has been undertaken some years ago in our laboratory with the aim to investigate the structural, morphological, electronic, magnetic, redox and catalytic properties of several oxide perovskite-type solid solutions. In previous papers, we have reported the results of our study on the LaMn_{1-x}Cu_xO₃, LaCo_{1-x}Cu_xO₃ [6,7], AMnO₃ (A = La, Nd, Sm), and Sm_{1-x}Sr_xMnO₃ systems [8]. This paper reports on the results of the research carried out on

* Corresponding author. Tel.: +39-06-49913378; fax: +39-06-490324.
E-mail address: piero.porta@uniroma1.it (P. Porta).

the AFeO_3 ($A = \text{La, Nd, Sm}$) and $\text{LaFe}_{1-x}\text{Mg}_x\text{O}_3$ perovskites, with the aim: (i) to understand the effect of the rare-earth A cation and/or of the cation substitution in the B sites on the ease of the perovskite-phase formation, and (ii) to find a correlation between the change in chemical composition with structural and redox properties.

2. Experimental procedure

AFeO_3 ($A = \text{La, Nd, Sm}$) and $\text{LaFe}_{1-x}\text{Mg}_x\text{O}_3$ ($x = 0.0, 0.1, 0.2, 0.3, 0.4, \text{ and } 0.5$) perovskite-type materials were prepared from citrate precursors [9]. A concentrated solution of metal nitrates was mixed with an aqueous solution of citric acid, by fixing at unity the molar ratio of citric acid to the total metal cations. Water was evaporated from the mixed solution at 353 K until a viscous gel was obtained. The gel was heated overnight at 383 K to yield a brownish vitreous material which was ground, heated at 423 K for 1 h and then slowly calcined at 623 K for 5 h. The samples, after grinding, were then calcined for 5 h each at 773, 923 and 1073 K, their characterization being performed at every step of firing. All the calcined AFeO_3 samples were ochre-yellow, whereas the Mg-containing lanthanum orthoferrites were dark-brown.

Inductively coupled plasma (ICP) emission spectroscopy was used to determine the rare-earth metal content. Atomic absorption (AA) spectroscopy was employed for magnesium and total iron content.

The amount of tetravalent iron was estimated by redox reaction: $\text{Fe}^{4+} + \text{Fe}^{2+} = 2\text{Fe}^{3+}$. A weighed amount of sample was dissolved in a known excess of standardized Mohr salt solution, followed by addition of a 4 N H_2SO_4 solution and back titration of the remaining Fe^{2+} equivalents with an N/10 $\text{K}_2\text{Cr}_2\text{O}_7$ solution, using ferroin as indicator. The titration was performed twice for each sample, the difference between the two determinations being in all cases within 5%.

Phase analysis, lattice parameters, and particle size determination were performed by X-ray diffraction (XRD) using a Philips PW 1729 diffractometer equipped with an IBM PS2 computer for data acquisition and analysis (software APD-Philips). Scans were taken with a 2θ step of 0.01° and using Ni-filtered $\text{Cu K}\alpha$ radiation. Lattice parameters were evaluated from all reflections appearing in the range of $2\theta = 20\text{--}60^\circ$, by means of the UNIT-CELL program [10]. Particle sizes were evaluated by means of the Scherrer equation $D = K\lambda/\beta \cos \theta$ after Warren's correction for instrumental broadening [11]. D is the mean crystallite diameter of the particles supposed spherical, K a constant equal to 0.9, λ the wavelength of the X-ray used, β the effective line width of the X-ray reflection under observation, calculated by the expression $\beta^2 = B^2 - b^2$ (where B is the full-width at half maximum (FWHM), b the instrumental broadening determined through the FWHM of the X-ray reflection at $\theta = 14^\circ$ of SiO_2 having particles larger than 1000 \AA , θ the diffraction angle of the X-ray reflection considered ($\theta = 16.25^\circ$ for Sm and Nd compounds, $\theta = 16.1^\circ$ for the La-perovskites).

The reduction of the materials was examined by XRD in an Anton-Paar camera, using Ni-filtered $\text{Cu K}\alpha$ radiation. The samples were heated in situ at 823 K for 1 h in a flow of 50 ml min^{-1} of H_2/N_2 mixture (6/94, v/v). After reduction, all the samples were ochre-yellow.

BET surface areas were measured by gas adsorption at 77 K, using krypton for samples fired at 1073 K and N_2 for those fired at lower temperatures, in a volumetric all glass apparatus.

Temperature programmed reduction (TPR) measurements were performed on the samples calcined at 923 K with a 2% H_2/Ar mixture ($25 \text{ cm}^3 \text{ min}^{-1}$) and a heating rate of 10 K min^{-1} up to 873 K, using a Micromeritics 2900 analyzer equipped with a TC detector and coupled with a Hiden HPR 20 mass spectrometer.

Diffuse reflectance spectra were taken in the wavelength range 200–800 nm ($50\,000\text{--}12\,500 \text{ cm}^{-1}$) with a Varian CARY 5E spectrometer equipped with an IBM PS2 computer for data acquisition and analysis and using PTFE as reference.

Magnetic susceptibility data were collected in the temperature range 100–300 K and at different magnetic-field strengths using the Gouy method. Correction was applied for the diamagnetism of the samples.

3. Results and discussion

Table 1 reports the chemical formula, the $\text{Fe}^{4+}/\text{Fe}_{\text{total}}$ ratio determined by TPR and redox titration, the Fe^{4+}/Mg ratio, and the values of lattice parameters, crystallite sizes and surface areas for the 923 K samples whose properties will be examined in more detail.

The nominal metal contents agreed within 5% with the experimental ones. The following experimental values were obtained (nominal content in parenthesis):

- $\text{LaFe}_{1-x}\text{Mg}_x\text{O}_3$: $x = 0.0$: La = 57.8 (57.2), Fe = 21.9 (23.0); $x = 0.1$: La = 56.1 (57.9), Fe = 20.2 (20.9), Mg = 1.06 (1.01); $x = 0.2$: La = 58.4 (58.7), Fe = 18.4 (18.9), Mg = 2.07 (2.05); $x = 0.3$: La = 57.3 (59.5), Fe = 16.0 (16.8), Mg = 2.96 (3.13); $x = 0.4$: La = 57.8 (60.3), Fe = 13.9 (14.5), Mg = 3.95 (4.23); $x = 0.5$: La = 58.1 (61.2), Fe = 12.0 (12.3), Mg = 5.09 (5.35).
- NdFeO_3 : Nd = 56.7 (58.1), Fe = 21.8 (22.5).
- SmFeO_3 : Sm = 56.9 (58.1), Fe = 21.8 (22.5).

The ease of the perovskite-phase formation from citrate precursors was checked by XRD analysis on samples calcined at different temperatures. Figs. 1–3 show the XRD patterns for the samples calcined at 623, 923 and 1073 K, respectively (the spectra for the samples heated at 773 K, similar to those reported in Fig. 1, are not reported). It may be noted that at the lowest temperature (623 K, Fig. 1) the perovskite structure is already formed for the LaFeO_3 , $\text{LaFe}_{0.9}\text{Mg}_{0.1}\text{O}_3$ and NdFeO_3 samples, whereas

Table 1

Orthoferrite perovskites obtained by calcination at 923 K for 5 h. Chemical formula, $ABO_{3\pm\delta}$, deduced from metal content (by ICP and AA) and Fe^{4+} concentration (by TPR); Fe^{4+}/Fe_{total} ratio estimated by TPR and chemical analysis (c.a.); Fe^{4+}/Mg ratio; lattice parameters a , b , c , V (with standard deviations in parenthesis); crystallite dimension D (Å); surface area, SA ($m^2 g^{-1}$)

Chemical formula	Fe^{4+}/Fe_{total}		Fe^{4+}/Mg	a (Å)	b (Å)	c (Å)	V (Å ³)	D	SA
	TPR	c.a.							
$SmFe_{0.068}^{4+}Fe_{0.932}^{3+}O_{3+0.034}$	0.068	0.057		5.588 (3)	7.710 (6)	5.392 (3)	232.3 (2)	328	8.0
$NdFe_{0.02}^{4+}Fe_{0.98}^{3+}O_{3+0.01}$	0.02	0.014		5.571 (3)	7.753 (8)	5.439 (5)	234.9 (2)	429	3.6
$LaFe_{0.024}^{4+}Fe_{0.976}^{3+}O_{3+0.012}$	0.024	0.032		5.554 (9)	7.863 (7)	5.560 (9)	242.8 (4)	352	12.4
$LaFe_{0.076}^{4+}Fe_{0.824}^{3+}Mg_{0.1}O_{3-0.012}$	0.084	0.08	0.76	5.556 (9)	7.859 (8)	5.560 (9)	242.7 (4)	364	8.2
$LaFe_{0.120}^{4+}Fe_{0.680}^{3+}Mg_{0.2}O_{3-0.040}$	0.15	0.15	0.60	5.557 (6)	7.848 (5)	5.528 (8)	241.1 (3)	302	4.2
$LaFe_{0.107}^{4+}Fe_{0.593}^{3+}Mg_{0.3}O_{3-0.096}$	0.15	0.16	0.36	5.556 (9)	7.857 (7)	5.543 (9)	242.0 (4)	272	n.d.
$LaFe_{0.094}^{4+}Fe_{0.506}^{3+}Mg_{0.4}O_{3-0.153}$	0.16	0.18	0.23	5.540 (9)	7.856 (7)	5.542 (9)	241.2 (4)	171	n.d.
$LaFe_{0.067}^{4+}Fe_{0.433}^{3+}Mg_{0.5}O_{3-0.216}$	0.13	0.15	0.13	5.554 (9)	7.850 (9)	5.539 (9)	241.5 (5)	156	n.d.

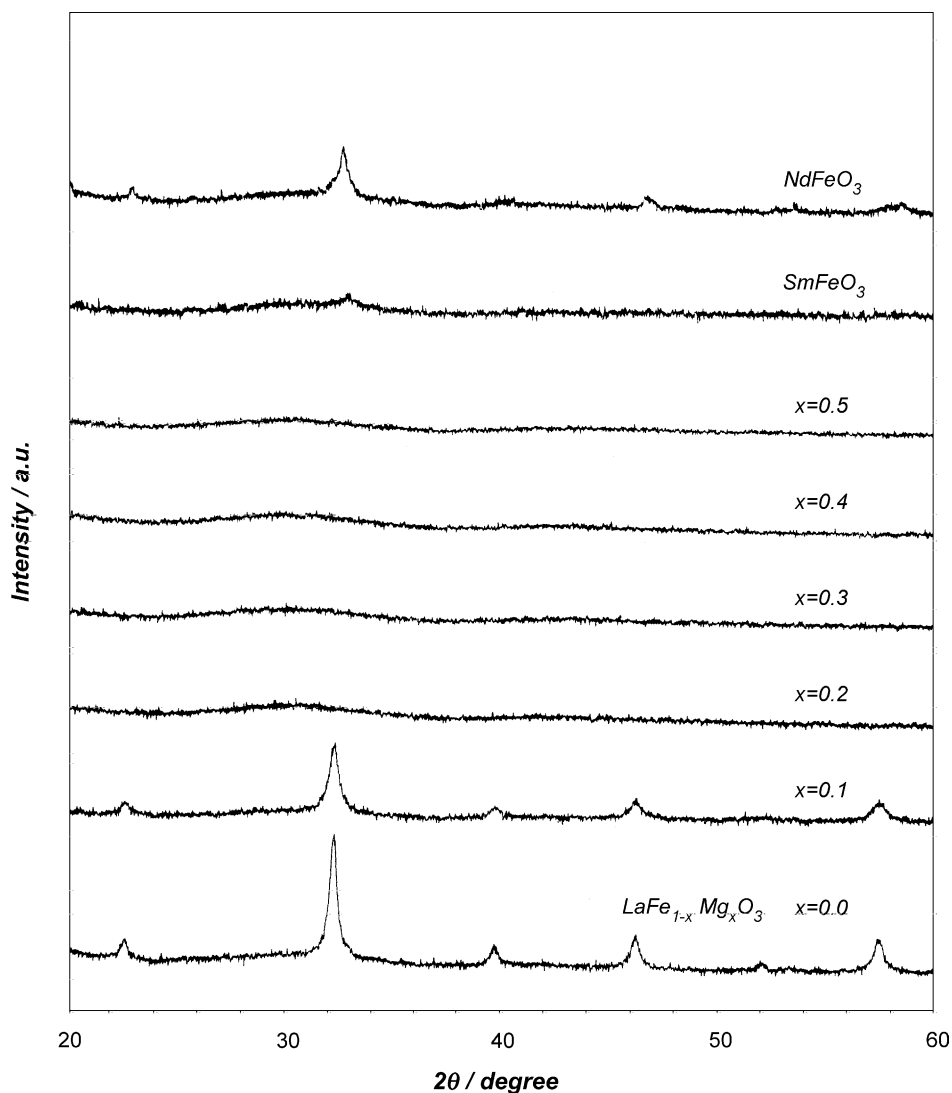


Fig. 1. XRD spectra for the $LaFeO_3$, $LaFe_{1-x}Mg_xO_3$, $SmFeO_3$ and $NdFeO_3$ samples calcined at 623 K.

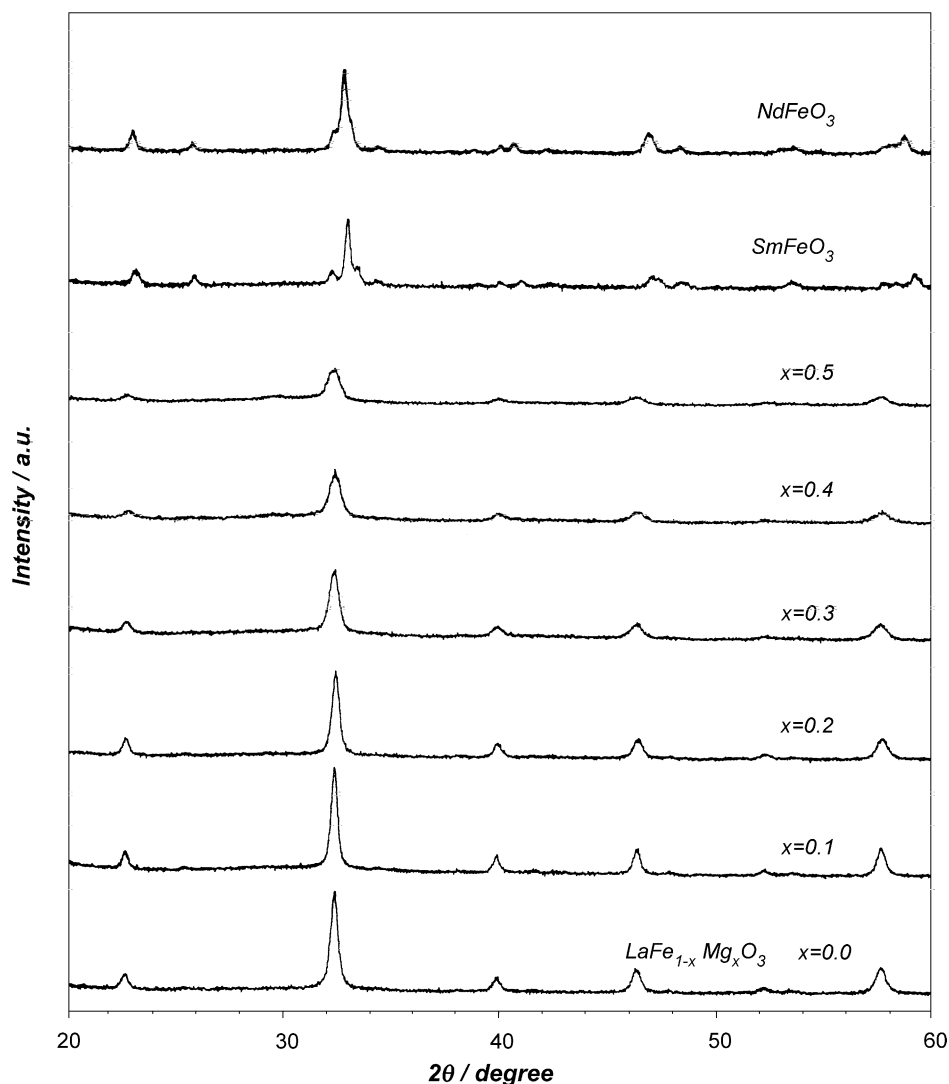


Fig. 2. XRD spectra for the LaFeO_3 , $\text{LaFe}_{1-x}\text{Mg}_x\text{O}_3$, SmFeO_3 and NdFeO_3 samples calcined at 923 K.

an amorphous phase is observed for all the other specimens. At 923 K (Fig. 2) and 1073 K (Fig. 3) a well-crystallized perovskite structure is evident for all the materials. Note that the $\text{LaFe}_{1-x}\text{Mg}_x\text{O}_3$ samples with $x = 0.4$ and 0.5 calcined at 1073 K (Fig. 3) revealed, in addition to a less crystalline perovskite phase, two very weak extra lines corresponding to the most intense X-ray reflections of La_2O_3 [12].¹ It may therefore be concluded that the perovskite phase is more easily obtained for LaFeO_3 , $\text{LaFe}_{0.9}\text{Mg}_{0.1}\text{O}_3$ and NdFeO_3 samples than either SmFeO_3 or $\text{LaFe}_{1-x}\text{Mg}_x\text{O}_3$ with $x > 0.1$. This feature will be later explained by taking into account the lattice parameters and reducibility trends.

The values of the mean crystallite diameter, D , as a function of the calcination temperature, for LaFeO_3 , $\text{LaFe}_{0.9}\text{Mg}_{0.1}\text{O}_3$, and NdFeO_3 are reported in Fig. 4. They reflect the trend of crystallinity observed on the relative

XRD patterns, and the behavior of D for all samples except NdFeO_3 at 773 K agrees with the opposite trend of surface areas also shown in Fig. 4.

The values of the lattice parameters, obtained from a least-squares refinement (the hkl indexes being assigned to the orthorhombic GdFeO_3 -type structure with $Pnma$, N.62, space group symmetry) [12],² are shown in Figs. 5 and 6 and in Table 1.

The binary SmFeO_3 , NdFeO_3 and LaFeO_3 perovskites show unit cell dimensions similar to those quoted in the XRD powder files [12] (see Footnote 2). The observed difference in the unit cell volume, V , agrees with that expected from the difference in size volume of the involved rare-earth ions (supposed spherical). In fact, the observed percent variation in unit cell volume between SmFeO_3 and NdFeO_3 is 1.1%,

¹ Files 5–602 for La_2O_3 .

² Files 39–1490 for SmFeO_3 ; 25–1149 for NdFeO_3 ; 37–1493 for LaFeO_3 .

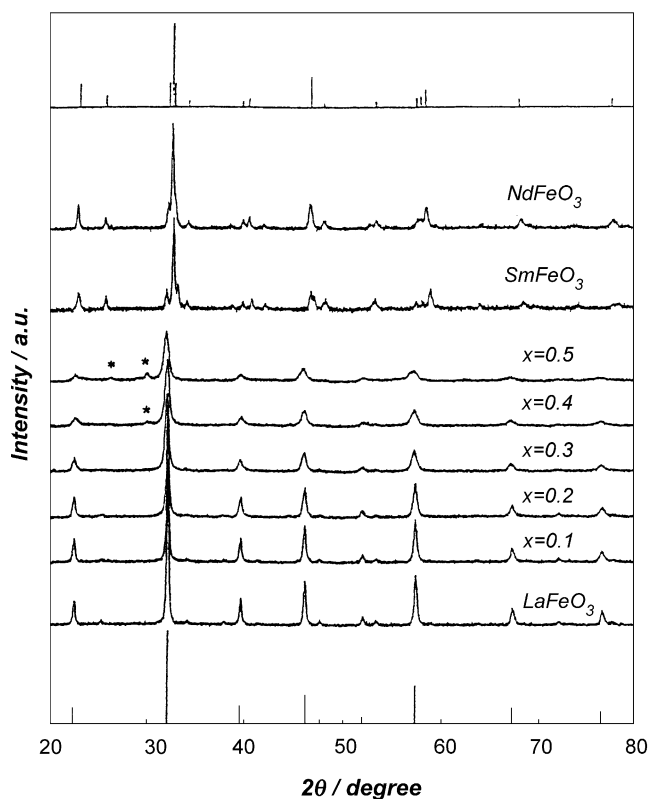


Fig. 3. XRD spectra for the LaFeO₃, LaFe_{1-x}Mg_xO₃, SmFeO₃ and NdFeO₃ samples calcined at 1073 K. Reference X-ray lines belonging to NdFeO₃ (12b) and to LaFeO₃ (12c) are given at the top and at the bottom, respectively. Asterisk corresponds to La₂O₃.

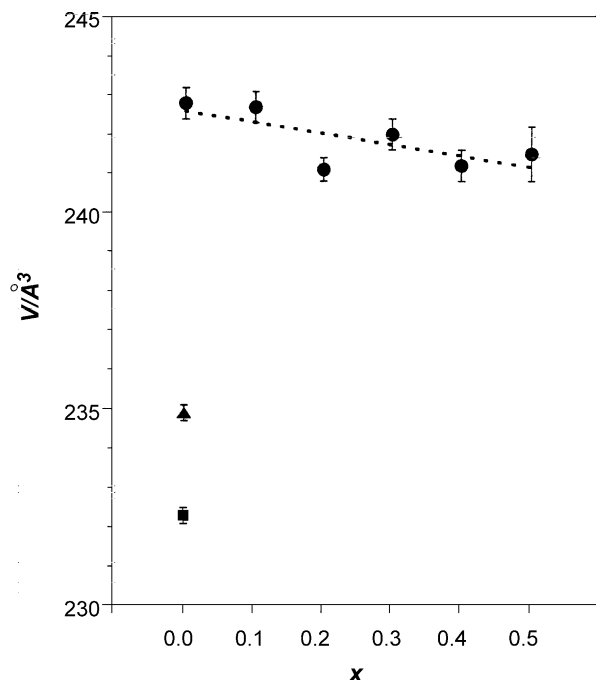


Fig. 5. Unit cell volume vs. substitution parameter x for the samples calcined at 923 K. Circle: LaFe_{1-x}Mg_xO₃; triangle: NdFeO₃; square: SmFeO₃. Bar corresponds to the estimated error.

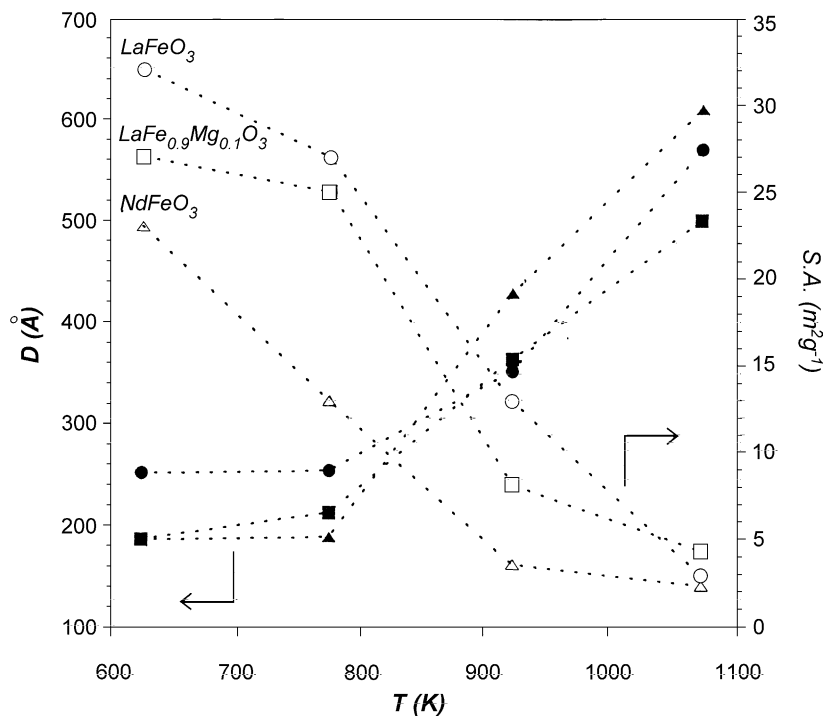


Fig. 4. Crystallite diameter, D (full symbol), and surface area, SA (open symbol) vs. calcination temperature, for LaFeO₃, LaFe_{0.9}Mg_{0.1}O₃ and NdFeO₃ samples.

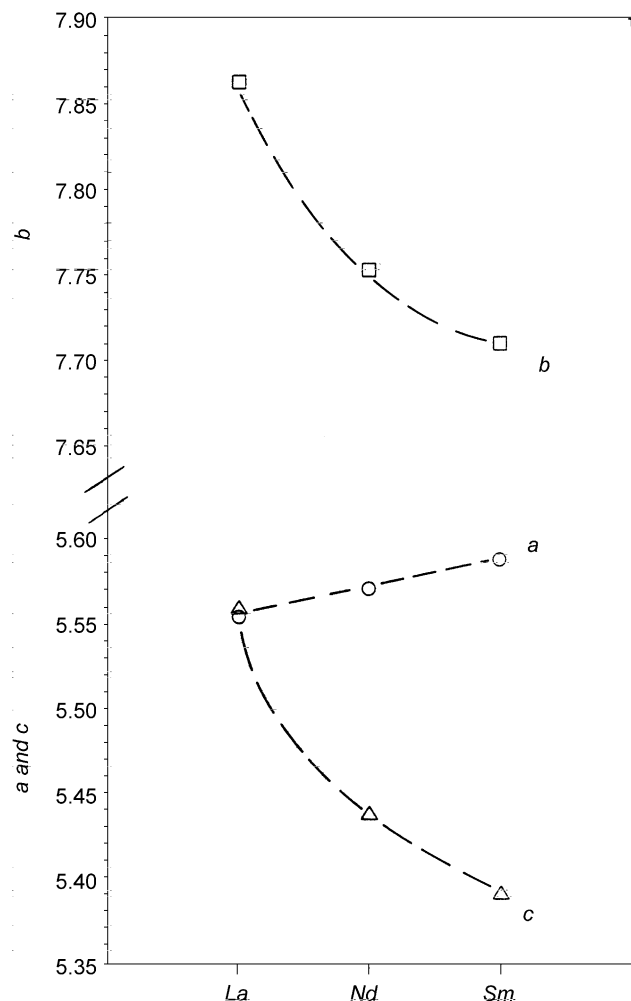


Fig. 6. Lattice parameters a , b , and c vs. x for the SmFeO_3 , NdFeO_3 , and LaFeO_3 samples calcined at 923 K. Circle: a ; triangle: c ; square: b .

and that between NdFeO_3 and LaFeO_3 is 3.3%, in accordance with the percent differences in size volume (1.0 and 3.2%, respectively) estimated from the relative ionic radii of the rare-earth ions in 12-coordination (Shannon's ionic radii: $r_{\text{Sm}^{3+}} = 1.24 \text{ \AA}$, $r_{\text{Nd}^{3+}} = 1.27 \text{ \AA}$, $r_{\text{La}^{3+}} = 1.36 \text{ \AA}$ [13]).

Fig. 6 clearly shows that by going from SmFeO_3 to LaFeO_3 through NdFeO_3 , a decreases slightly, whereas both b and c increase in such a way that, in LaFeO_3 , c approaches the value of a , and b (7.863 Å) is equal to the double length of the cubic pseudo-cell dimension which, according to Geller and Wood [14] is estimated as 3.932 Å. With the increase in size of the A ion ($r_{\text{Sm}^{3+}} < r_{\text{Nd}^{3+}} < r_{\text{La}^{3+}}$), the lattice seems therefore to approach the cubic ideal perovskite structure.

Note that Marezio and Dernier, in a single-crystal XRD study [15], gave evidence that samarium in SmFeO_3 has coordination number equal to 8, with eight first nearest and four second nearest oxygen atoms, whereas a progressively lower distortion of the A-oxygen polyhedron was observed in NdFeO_3 and LaFeO_3 . On the other hand, the same authors reported that the iron octahedron across the rare-earth

orthoferrite series is only slightly distorted, so approaching the ideal cubic arrangement within the B-sublattice. The average Fe–O distance within the Fe-octahedron of LaFeO_3 was given by the same authors as 2.006 Å.

The average A–O and Fe–O distances may be estimated from the cell size of the idealized cubic lattice ($\frac{1}{2}b$ of the orthorhombic cell) [14]. By taking into account the observed $\frac{1}{2}b$ values reported in Table 1 (3.874, 3.889 and 3.932 Å for SmFeO_3 , NdFeO_3 and LaFeO_3 , respectively), the corresponding estimated interionic distances ($\text{A–O} = \frac{1}{4}b\sqrt{2}$, $\text{Fe–O} = \frac{1}{4}b$) are, for SmFeO_3 , NdFeO_3 and LaFeO_3 , respectively: $\text{Sm–O} = 2.74 \text{ \AA}$, $\text{Nd–O} = 2.75 \text{ \AA}$, and $\text{La–O} = 2.78 \text{ \AA}$; $\text{Fe–O} = 1.937$, 1.945 , and 1.966 \AA .

Note that the estimated A–O distances are slightly longer than those expected ($\text{Sm–O} = 2.64 \text{ \AA}$, $\text{Nd–O} = 2.67 \text{ \AA}$, $\text{La–O} = 2.76 \text{ \AA}$) on the basis of the sum of the ionic radii (rare-earth ions in CN = 12: $r_{\text{Sm}^{3+}} = 1.24 \text{ \AA}$, $r_{\text{Nd}^{3+}} = 1.27 \text{ \AA}$, $r_{\text{La}^{3+}} = 1.36 \text{ \AA}$; oxygen in CN = 6: $r_{\text{O}^{2-}} = 1.40 \text{ \AA}$ [13]).

On the other hand, the estimated Fe–O distances are much shorter than the value (2.045 Å) expected on the basis of the sum of the ionic radii ($r_{\text{Fe}^{3+}} = 0.645 \text{ \AA}$ for high spin (HS) electron configuration in octahedral coordination, $r_{\text{O}^{2-}} = 1.40 \text{ \AA}$ [13]). This feature may suggest that a certain degree of covalence is present in the Fe–O bonds, whose nature may also depend on the type of the partner A rare-earth ion. The presence of some smaller Fe^{4+} species ($r_{\text{Fe}^{4+}} = 0.585 \text{ \AA}$ in CN = 6 [13]) derived from TPR measurements and redox titration, may of course contribute to lower the observed Fe–O distance. However, the amount of Fe^{4+} detected in the binary AFeO_3 perovskites is small (in the range 2–6%, see Table 1), and, moreover, the expected $\text{Fe}^{4+}\text{–O}$ distance (1.985 Å [13]) is still higher than the evaluated Fe–O distances.

The Fe–O bond strength should be considered as relevant, in our opinion, when a correlation is looked for between some chemical properties, such as catalytic performance, and structural ones of the AFeO_3 perovskites. The redox properties of the materials and their catalytic behavior may be linked, for instance, to their structural characteristics. If lattice oxygen, in addition to the surface one, of the perovskite catalyst is involved in oxidation reactions, less reducible materials (having stronger Fe–O bonds and oxygen more strongly bonded) should in principle correspond to less active catalysts, for instance, for deep oxidation of hydrocarbons. Note that catalytic tests of methane combustion performed by us on the AFeO_3 materials showed that the trend of activity ($\text{SmFeO}_3 < \text{NdFeO}_3 < \text{LaFeO}_3$ [16]) in the lower temperature region of reaction, fits well their tendency to reduction shown in the following paragraphs.

TPR patterns of SmFeO_3 , NdFeO_3 and LaFeO_3 calcined at 923 K are reported in Fig. 7. For SmFeO_3 a peak with maximum at 690 K is present, whereas NdFeO_3 shows two distinct reduction peaks with maxima at 530 and 650 K, respectively. The corresponding peak for LaFeO_3 with max-

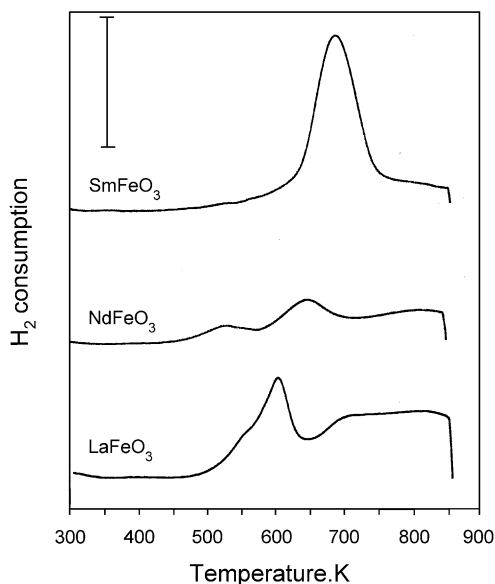


Fig. 7. TPR profiles for LaFeO_3 , NdFeO_3 and SmFeO_3 perovskites calcined at 923 K. Bar corresponds to $1 \mu\text{mol H}_2 \text{g}^{-1} \text{K}^{-1}$.

imum at 590 K shows a shoulder at lower temperature (a large band is also visible in the higher temperature region of the spectrum). The TPR peaks correspond to the reduction of some fraction of Fe^{4+} within the perovskites. The trend of decreasing temperature of the reduction by going from Sm- to Nd- and to La-orthoferrite thus agrees with the increase in the estimated bond distances ($\text{Fe}-\text{O} = 1.937$, 1.945 and 1.966 \AA for SmFeO_3 , NdFeO_3 and LaFeO_3 , respectively), and, therefore, with the decrease of the overall $\text{Fe}-\text{O}$ bond strength. Note, moreover, that $\text{Fe}^{4+}/\text{Fe}_{\text{total}}$ ratio, evaluated by redox titration and TPR hydrogen uptake, indicates that the presence of Fe^{4+} in the AFeO_3 materials is compensated by a small cation defectivity, as described by the oxidative non-stoichiometric, $\text{ABO}_{3+\delta}$, chemical formulae reported in Table 1.

Regarding $\text{LaFe}_{1-x}\text{Mg}_x\text{O}_3$ solid solutions, a slight decrease (with a small minimum at $x = 0.2$) of the unit cell volume, V , at the increase of x was observed (Fig. 5).

To explain such behavior and to derive the chemical composition of the samples, let us consider the results of redox titration and TPR experiments. TPR profiles for samples calcined at 923 K are reported in Fig. 8. They show the presence of a main peak with the maximum placed at progressively increasing temperature (except for the sample with $x = 0.3$) with the increase of magnesium content. The samples thus seem to be less and less reducible with increasing magnesium content.

The TPR peak corresponds, as for the AFeO_3 samples, to the reduction of the fraction of Fe^{4+} (compensating the lower charge of Mg^{2+}) to Fe^{3+} . However, the amount of Fe^{4+} , evaluated from chemical titration and hydrogen uptake by TPR, and consequently the value of the $\text{Fe}^{4+}/\text{Mg}^{2+}$ ratio (Table 1), is lower than that necessary to the charge balance.

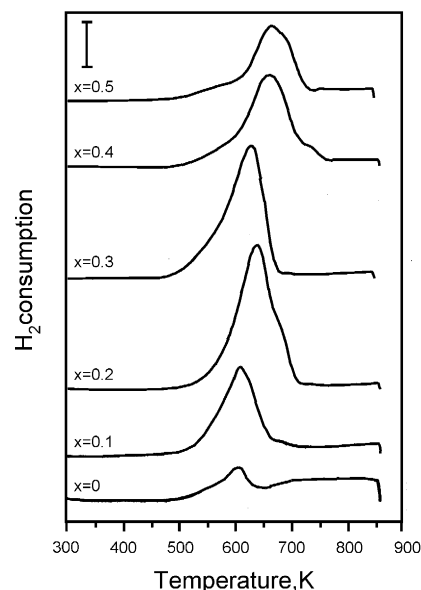


Fig. 8. TPR profiles for $\text{LaFe}_{1-x}\text{Mg}_x\text{O}_3$ perovskites calcined at 923 K. Bar corresponds to $1 \mu\text{mol H}_2 \text{g}^{-1} \text{K}^{-1}$.

Therefore, oxygen vacancies should compensate the positive charge defectivity for these samples. Table 1 reports the oxygen defective, $\text{ABO}_{3-\delta}$, chemical formulae derived for each sample on the basis of the Fe^{4+} content.

At the light of the obtained results, the variation of the unit cell volume shown in Fig. 5 may be interpreted as the consequence of the combined effect of the substitution in the perovskite octahedral B sublattice of larger Mg^{2+} (0.72 \AA) and smaller Fe^{4+} (0.585 \AA) for Fe^{3+} -HS ions (0.645 \AA) [13]. The tendency to decrease in the cell volume seems to indicate that the latter effect prevails on the former one.

Note that an XRD analysis performed on all the samples after the TPR experiment, as well as on samples reduced in situ at 823 K in the Anton-Paar XRD camera, showed: (i) the persistence of the perovskite structure without any detected extra phase, and (ii) a clear displacement of all the X-ray reflections towards lower 2θ angles. Point (ii), i.e. the observed unit cell expansion is mainly justified by the higher content of larger Fe^{3+} ions. Moreover, the absence of extra phases such as MgO seems to indicate that in the reduced $\text{LaFe}_{1-x}\text{Mg}_x\text{O}_3$ perovskites the positive charge defectivity is compensated by a higher amount of oxygen vacancies. Note also that all the samples after TPR or reduction in the Anton-Paar XRD camera, changed in color from dark-brown to ochre-yellow, the latter color being typical of many inorganic compounds containing Fe^{3+} species.

From the lattice parameter and TPR results, it is now possible to explain why the perovskite phase is more easily obtained for LaFeO_3 , $\text{LaFe}_{0.9}\text{Mg}_{0.1}\text{O}_3$ and NdFeO_3 samples than either SmFeO_3 or $\text{LaFe}_{1-x}\text{Mg}_x\text{O}_3$ solid solutions with $x > 0.1$. The lattice distortion and perturbation caused by samarium tend indeed to hinder the formation of SmFeO_3 , and the contemporary presence of bigger Mg^{2+}

ions, octahedrally distorted (by large Jahn–Teller effect) Fe^{4+} species [17], and increasing oxygen defectivity in the $\text{LaFe}_{1-x}\text{Mg}_x\text{O}_3$ solid solutions, contributes to impede the formation at lower temperature of the perovskite phase in the high Mg-containing lanthanum orthoferrites.

Reflectance spectroscopy is a useful tool to draw information on the electronic properties of materials where ionic species with open-shell configuration are present. Fe^{3+} has normally an HS configuration with five unpaired electrons in the 3d orbitals. The free ion ground term ${}^6\text{S}$ state, $[(t_{2g})^3(e_g)^2]$, gives rise, in an octahedral field, to the ${}^4\text{T}_{1g}$, ${}^4\text{T}_{2g}$, ${}^4\text{A}_{1g}$, ${}^4\text{A}_{2g}$, and ${}^4\text{E}_g$ quartet states. In the octahedral $[\text{Fe}(\text{H}_2\text{O})_6]^{3+}$ ion the band transitions from the ground term occur at 12 600, 18 500, 24 300 and 24 600 cm^{-1} [18,19].

Fe^{4+} in the $[(t_{2g})^3(e_g)^1]$ electron configuration is dominated by charge transfer absorption and is expected to present weak transition bands in the near infrared or visible region [18,19].

La^{3+} in the $4f^0$ state is spectroscopically silent, whereas Nd^{3+} and Sm^{3+} having, respectively, $4f^3$ and $4f^5$ unfilled electron shell configuration should present only very weak bands in the UV spectral region [18,19]. From theoretical expectations, it may be concluded that the optical spectra of our samples should be diagnostic only for the Fe^{3+} species.

The optical bands, shown in Fig. 9, occur for the AFeO_3 samples at about 13 000, 18 800, 21 500, 27 000, 32 000 and

41 700 cm^{-1} and are those expected for d–d and ligand to metal charge transfer transitions of Fe^{3+} in octahedral coordination [18,19]. For the $\text{LaFe}_{1-x}\text{Mg}_x\text{O}_3$ materials the spectra exhibit a very poor resolution mainly because of the darkness of the samples (presence of Fe^{4+}). In fact, for the reduced $\text{LaFe}_{1-x}\text{Mg}_x\text{O}_3$ samples, where the color changed to ochre-yellow (from dark-brown, before reduction), the spectra appeared highly resolved (an example is given in Fig. 9 for the $\text{LaFe}_{0.7}\text{Mg}_{0.3}\text{O}_3$ material after reduction).

Magnetic susceptibility measurements performed at various temperatures offer a further tool to determine the oxidation state of paramagnetic species present in the solids and to evidence the occurrence of magnetic interactions between them.

The magnetic properties of rare-earth orthoferrites are very interesting and have been extensively studied by Néel and his school [20,24–26] in the past, and subsequently by other authors [21,22]. Rare-earth orthoferrites are essentially antiferromagnetic, but tend to exhibit a weak parasitic ferromagnetism, which is an intrinsic property of the iron sublattice of the perovskite structure and disappears at a temperature of about 700 K (mean Néel temperature of the iron sublattice in several perovskites). As pointed out by Goodenough [22], the weak parasitic ferromagnetism observed in the rare-earth orthoferrites is due to one or more of the following contributions: (i) preferential ordering of impurities or defects into alternate (1 1 1) planes of the antiferromagnetic iron octahedral sublattice, (ii) interstitial Fe ions in inhomogeneity-induced regions of high iron concentration, (iii) Fe^{3+} spins canted in a common direction mainly by anisotropic superexchange, and (iv) canting of the antiferromagnetic rare-earth sublattice due to the interactions between the two 12-coordinated and octahedral sublattices. By means of thermomagnetic analysis it was also found that the ferromagnetic properties of orthoferrites are influenced by the size of the rare-earth ion [20,24–26].

Fig. 10 shows the inverse atomic magnetic susceptibility, χ_{at}^{-1} versus T , for SmFeO_3 and NdFeO_3 (a) and for some $\text{LaFe}_{1-x}\text{Mg}_x\text{O}_3$ (b) perovskites. The results for Nd_2O_3 are also reported in Fig. 10(a). In agreement with the literature [21], Nd_2O_3 shows a paramagnetic behavior with an effective magnetic moment μ equal to $3.47\mu_B$ and a Curie temperature θ of -30 K. A similar feature is displayed by NdFeO_3 which follows the Curie–Weiss law with a θ value of -80 K and an effective magnetic moment μ of $3.88\mu_B$. On the other hand, as expected for the temperature range used by us (well below the Néel temperature of about 700 K), both SmFeO_3 (Fig. 10(a)) and LaFeO_3 (Fig. 10(b)) exhibit a non-paramagnetic behavior. Note that a behavior similar to that observed by us for LaFeO_3 has been reported for the $\text{LaFe}_{0.9}\text{Ni}_{0.1}\text{O}_3$ mixed perovskite [23]. The introduction of magnesium in LaFeO_3 seems to reduce the strength of magnetic interactions in the iron sublattice so that, as shown in Fig. 10(b) for the $\text{LaFe}_{1-x}\text{Mg}_x\text{O}_3$ samples with $x = 0.2$ and 0.5 , the $\chi_{\text{at}}^{-1}-T$ plots tend to approach the typical paramagnetic behavior.

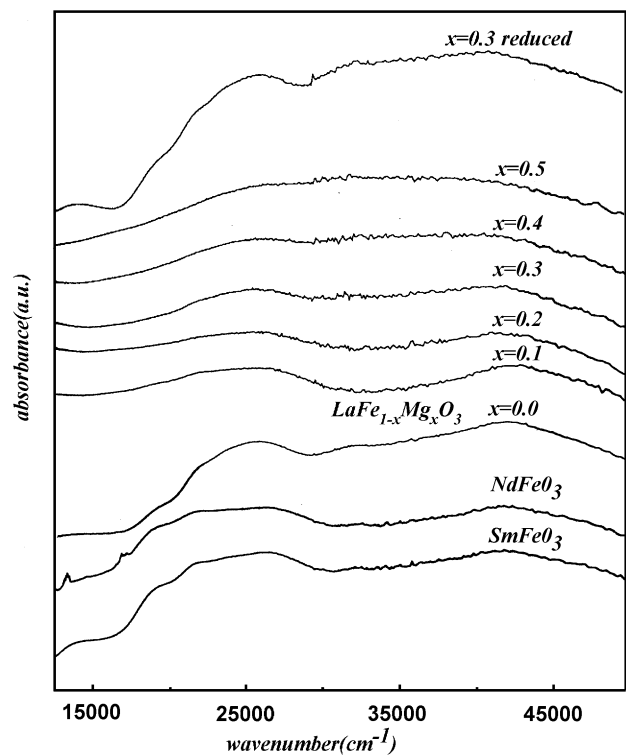


Fig. 9. Reflectance spectra for SmFeO_3 , NdFeO_3 , and $\text{LaFe}_{1-x}\text{Mg}_x\text{O}_3$ samples. The spectrum of $\text{LaFe}_{1-x}\text{Mg}_x\text{O}_3$ with $x = 0.3$ after XRD in situ reduction is reported at the top.

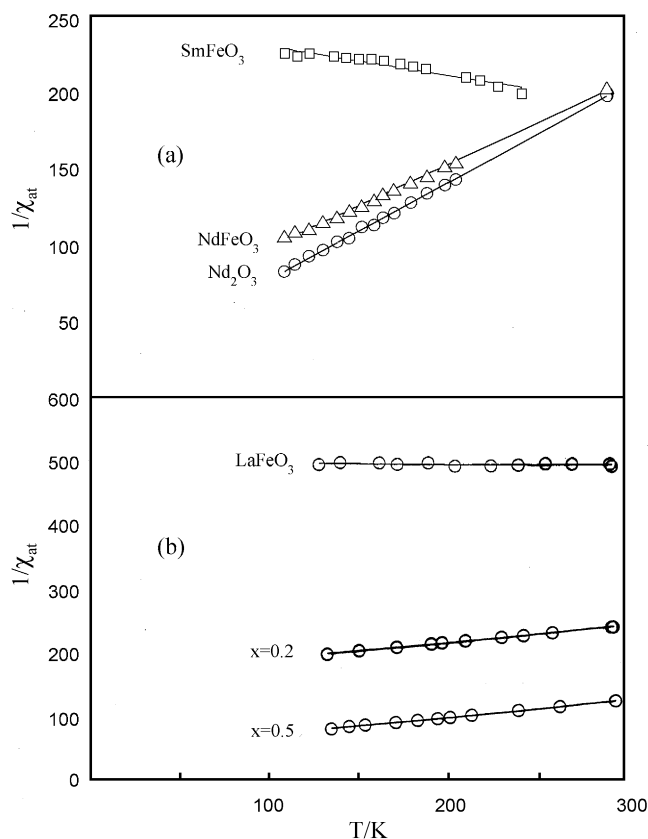


Fig. 10. Inverse of atomic magnetic susceptibility, χ_{at}^{-1} vs. temperature: (a) for SmFeO_3 , NdFeO_3 and Nd_2O_3 ; (b) for LaFeO_3 , and for $\text{LaFe}_{1-x}\text{Mg}_x\text{O}_3$ with $x = 0.2$ and 0.5 .

4. Conclusions

The change of the rare-earth cation in AFeO_3 ($A = \text{La}, \text{Nd}, \text{Sm}$) and the substitution of iron by magnesium in $\text{LaFe}_{1-x}\text{Mg}_x\text{O}_3$ perovskites give the following features:

1. Perovskites with less disordered structure (LaFeO_3 , $\text{LaFe}_{0.9}\text{Mg}_{0.1}\text{O}_3$, and NdFeO_3) can be more easily obtained than that (SmFeO_3) with a more distorted A-oxygen polyhedron, and those ($\text{LaFe}_{1-x}\text{Mg}_x\text{O}_3$ with $x > 0.1$) where a higher lattice perturbation caused by larger Mg^{2+} ions, octahedrally distorted Fe^{4+} ions, and anion defectivity, is present.
2. Fe^{4+} is present in SmFeO_3 , NdFeO_3 and LaFeO_3 binary perovskites, its content being compensated by cation defectivity.
3. $\text{Fe}^{4+}/\text{Mg}^{2+}$ ratio in $\text{LaFe}_{1-x}\text{Mg}_x\text{O}_3$ is lower than that necessary to charge compensation, so that oxygen vacancies counterbalance the positive charge defectivity.
4. After reduction, the perovskite structure is preserved with an expansion of the unit cell (specially observed in $\text{LaFe}_{1-x}\text{Mg}_x\text{O}_3$) due to higher content of larger Fe^{3+} ions.
5. The order of reducibility in AFeO_3 perovskites, $\text{LaFeO}_3 > \text{NdFeO}_3 > \text{SmFeO}_3$, and the decreasing

reducibility of the $\text{LaFe}_{1-x}\text{Mg}_x\text{O}_3$ solid solutions at the increase of x , are correlated with the increase in the relative Fe–O bond strengths, which implies oxygen more strongly bonded in SmFeO_3 , and in those $\text{LaFe}_{1-x}\text{Mg}_x\text{O}_3$ materials containing higher fraction of Fe^{4+} and anion vacancies.

6. The magnetic behavior confirms the interesting properties already found in SmFeO_3 , NdFeO_3 and LaFeO_3 perovskites. For $\text{LaFe}_{1-x}\text{Mg}_x\text{O}_3$ perovskites, the introduction of magnesium seems to perturb the ferromagnetic interactions within the iron octahedral sublattice.

References

- [1] L.G. Tejuca, J.L.G. Fierro (Eds.), Properties and Applications of Perovskite-type Oxides, Marcel Dekker, New York, 1993.
- [2] R.E. Newman, in: A. Navrotsky, D.J. Weidner (Eds.), Structure–Property Relationship in Perovskite Electroceramics. Perovskite: A Structure of Great Interest to Geophysics and Material Science, American Geophysical Union, Washington, DC, 1989.
- [3] V.M. Goldschmidt, Akad. Oslo. J. Mat. Natur. 2 (1926) 7.
- [4] L.J. Tejuca, J. Less Common Met. 146 (1988) 261.
- [5] R.J.H. Voorhoeve, D.W. Johnson Jr., J.P. Remeika, P.K. Gallagher, Science 195 (1977) 827.
- [6] P. Porta, S. De Rossi, M. Faticanti, G. Minelli, I. Pettiti, L. Lisi, M. Turco, J. Solid State Chem. 146 (1999) 291.
- [7] L. Lisi, G. Bagnasco, P. Ciambelli, S. De Rossi, P. Porta, G. Russo, M. Turco, J. Solid State Chem. 146 (1999) 176.
- [8] P. Ciambelli, S. Cimino, S. De Rossi, M. Faticanti, L. Lisi, G. Minelli, I. Pettiti, P. Porta, G. Russo, M. Turco, Appl. Catal. B 24 (2000) 243.
- [9] B. Delmon, J. Droguest, Belgium Patent 735476, September 15, 1969, Fine particles, in: W.H. Fuhr (Ed.), Second International Conference, The Electrochemical Society, p. 242.
- [10] T.J.B. Holland, S.A.T. Redfern, J. Appl. Crystallogr. 30 (1997) 84.
- [11] H.P. Klug, L.E. Alexander, X-ray Diffraction Procedures for Polycrystalline and Amorphous Materials, Wiley, London, 1962, p. 492.
- [12] Powder Diffraction File, Inorganic Volume, American Society for Testing Materials, Philadelphia, PA, 1967.
- [13] R.D. Shannon, Acta Crystallogr., Sect. A 32 (1976) 751.
- [14] S. Geller, E.A. Wood, Acta Crystallogr. 9 (1956) 563.
- [15] M. Marezio, P.D. Dernier, Mater. Res. Bull. 6 (1971) 23.
- [16] P. Ciambelli, S. Cimino, S. De Rossi, L. Lisi, G. Minelli, P. Porta, G. Russo, Appl. Catal. B 29 (2001) 239.
- [17] J.D. Dunitz, L.E. Orgel, J. Phys. Chem. Solids 3 (1957) 20.
- [18] A.B.P. Lever, Inorganic Electron Spectroscopy, 2nd Edition, Elsevier, Amsterdam, 1984.
- [19] C.K. Jorgensen, Absorption Spectra and Chemical Bonding in Complexes, Pergamon Press, Oxford, 1962.
- [20] L. Néel, C.R. Acad. Sci., Paris 239 (1954) 8.
- [21] M. Schieber, Experimental Magnetochemistry, North-Holland, Amsterdam, 1967, p. 309, and other references therein.
- [22] J.B. Goodenough, Magnetism and the Chemical Bond, Wiley, New York, 1963, p. 237, and other references therein.
- [23] N.Y. Vasanthacharya, P. Ganguly, C.N.R. Rao, J. Solid State Chem. 53 (1984) 140.
- [24] R. Pauthenet, P. Blum, C.R. Acad. Sci., Paris 239 (1954) 33.
- [25] G. Guiot-Guillain, C.R. Acad. Sci., Paris 237 (1953) 1654.
- [26] M.A. Gilleo, J. Chem. Phys. 24 (1956) 1239.